nature nanotechnology

LETTERS

PUBLISHED ONLINE: 2 FEBRUARY 2014 | DOI: 10.1038/NNANO.2014.2

Universal control and error correction in multi-qubit spin registers in diamond

T. H. Taminiau[1], J. Cramer[1], T. van der Sar[1†], V. V. Dobrovitski[2] and R. Hanson[1*]

Quantum registers of nuclear spins coupled to electron spins of individual solid-state defects are a promising platform for quantum information processing[1–13]. Pioneering experiments selected defects with favourably located nuclear spins with particularly strong hyperfine couplings[4–10]. To progress towards large-scale applications, larger and deterministically available nuclear registers are highly desirable. Here, we realize universal control over multi-qubit spin registers by harnessing abundant weakly coupled nuclear spins. We use the electron spin of a nitrogen–vacancy centre in diamond to selectively initialize, control and read out carbon-13 spins in the surrounding spin bath and construct high-fidelity single- and two-qubit gates. We exploit these new capabilities to implement a three-qubit quantum-error-correction protocol[14–17] and demonstrate the robustness of the encoded state against applied errors. These results transform weakly coupled nuclear spins from a source of decoherence into a reliable resource, paving the way towards extended quantum networks and surface-code quantum computing based on multi-qubit nodes[11,18,19].

Electron and nuclear spins associated with defects in solids provide natural hybrid quantum registers[3–11]. Fully-controlled registers of multiple spins hold great promise as building blocks for quantum networks[18] and fault-tolerant quantum computing[19]. The defect electron spin enables initialization and readout of the register and coupling to other (distant) electron spins[11,18], whereas the nuclear spins provide well-isolated qubits and memories with long coherence times[8,9,11]. Previous experiments relied on selected defects having nuclear spins with strong hyperfine couplings that exceed the inverse of the electron spin dephasing time ($1/T_2^*$). With these strongly coupled spins, single-shot readout[9,10,20–22] and entanglement[9,11] have been demonstrated. However, the number of strongly coupled spins varies per defect and is intrinsically limited, so universal control has so far been restricted to two-qubit registers[4,7] and the required control of multi-qubit registers has remained an open challenge.

Here, we overcome this challenge by demonstrating universal control of weakly coupled nuclear spins (unresolved hyperfine coupling $\ll 1/T_2^*$). We use the electron spin of single nitrogen–vacancy (NV) centres in room-temperature diamond to selectively control multiple carbon-13 (^{13}C) nuclear spins in the surrounding spin bath (Fig. 1a). With this new level of control we realize multi-qubit registers by constructing high-fidelity unconditional and electron-controlled gates, implementing initialization and readout and creating nuclear–nuclear entangling gates through the electron spin. Finally, we demonstrate the power of this approach by implementing the first quantum-error-correction protocol with individual solid-state spins.

We have used dynamical decoupling spectroscopy[23–25] to characterize the nuclear spin environment of a total of three NV centres, including one with an additional strongly coupled ^{13}C spin (see Supplementary Information). To demonstrate the generality of our approach to create multi-qubit registers, we realized the initialization, control and readout of three weakly coupled ^{13}C spins for each NV centre studied (see Supplementary Information). In the following, we consider one of these NV centres in detail and use two of its weakly coupled ^{13}C spins to form a three-qubit register for quantum error correction (Fig. 1a).

Our control method exploits the dependence of the nuclear spin quantization axis on the electron spin state as a result of the anisotropic hyperfine interaction (see Methods for hyperfine parameters), so no radiofrequency driving of the nuclear spins is required[7,23–28]. All nuclear gates are implemented by pulse sequences of the form $(\tau - \pi - 2\tau - \pi - \tau)^{N/2}$ where π is a microwave π-pulse on the electron spin, 2τ is the inter-pulse delay and N is the total number of pulses in the sequence. Each nuclear spin is controlled by precisely choosing τ in resonance with that spin's particular hyperfine interaction. The target spin, the type of gate (conditional or unconditional) and the rotation axis (X- or Z-rotation) are determined by the value of τ, and the total rotation angle is determined by N (see Methods). Crucially, at the same time, these sequences decouple the electron from the other nuclear qubits and the environment[7]. These decoherence-protected gates are selective and allow the full electron coherence time T_{coh} to be exploited ($T_{coh} = 2.86(4)$ ms, Fig. 1b). The gates are thus not limited by the electron spin dephasing time $T_2^* = 3.3(1)$ μs or the Hahn echo time T_2 and do not require strong coupling.

To initialize the nuclear spins we first prepare the electron spin in $m_s = 0$ by optical pumping (see Supplementary Information), then swap the electron state onto the nuclear spin, and finally re-initialize the electron spin (Fig. 1c). We characterize the nuclear initialization by preparing the electron spin in a superposition state and letting it evolve in a Ramsey-type experiment. Without initialization, a single-frequency oscillation with a Gaussian decaying envelope is observed, confirming that the NV centre feels a decohering bath of weakly coupled spins (Fig. 1d). Initializing the nuclear spins in the $|0\rangle$ ($|1\rangle$) state (Fig. 1d,e), we increase (decrease) the oscillation frequency because the magnetic field at the electron is enhanced (reduced) due to the hyperfine interaction. The oscillations also persist longer as quasistatic fluctuations of the two nuclear spins are suppressed[29], increasing the electronic dephasing time to $T_2^* = 4.0(2)$ μs. Initializing spin 1 has a more pronounced effect because spin 1 has a larger parallel component of the hyperfine interaction ($A_{\parallel}^1 = 2\pi \times 78.2(8)$ kHz) than spin 2 ($A_{\parallel}^2 = 2\pi \times 32(3)$ kHz). From such measurements, we obtain state initialization fidelities of $F_1 = 0.91(2)$ and $F_2 = 0.88(5)$ for nuclear spins 1 and 2, respectively (see Methods).

We next demonstrate the measurement of the individual nuclear spin states and verify that we observe two distinct ^{13}C

[1]Kavli Institute of Nanoscience, Delft University of Technology, PO Box 5046, 2600 GA Delft, The Netherlands, [2]Ames Laboratory and Iowa State University, Ames, Iowa 50011, USA; [†]Present address: Department of Physics, Harvard University, Cambridge, Massachusetts 02138, USA.
*e-mail: r.hanson@tudelft.nl

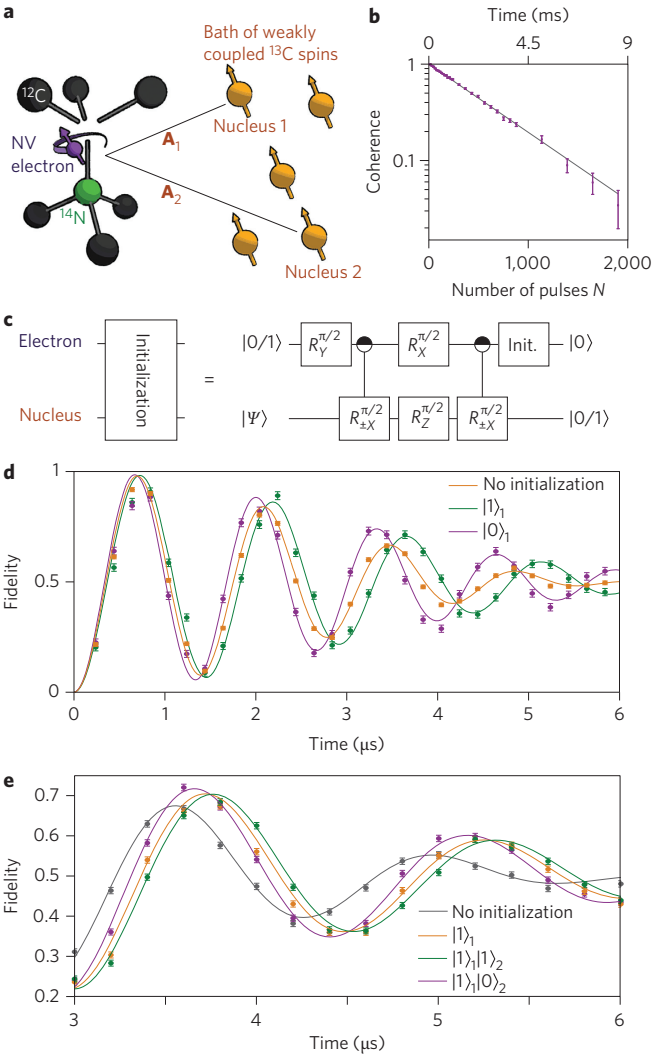

Figure 1 | Definition and initialization of the quantum registers. **a**, Quantum register formed by the NV electron spin ($S=1$; $|0\rangle=|m_s=0\rangle$, $|1\rangle=|m_s=-1\rangle$) and weakly coupled ^{13}C nuclear spins ($I=1/2$; state $|\psi\rangle_i$ and hyperfine interaction $\mathbf{A}_i$ for nuclear spin i; see Methods for values). All gates on nuclear spins are implemented by sequences of N π-pulses on the electron spin spaced by a time 2τ (see Methods). **b**, Electronic coherence as a function of total sequence length. The number of π-pulses N is increased for fixed $\tau=2\pi/\omega_L$, which is representative for our gates ($\omega_L=2\pi\times$ 431 kHz is the ^{13}C Larmor frequency). The $1/e$ time is $T_{coh}=2.86(4)$ ms. **c**, Nuclear spin initialization by swapping the electron state, $|0/1\rangle=|0\rangle$ or $|1\rangle$, onto the nuclear spin. The controlled gates ($R_{\pm X}^{\pi/2}$) are X-rotations by $\pi/2$ with a direction conditional on the electron spin state (see Methods). The final electron spin re-initialization by a 2 μs laser pulse (labelled 'Init.') preserves the nuclear spin polarization (T_1 values under illumination: 2.5(3) ms for nuclear spin 1 and 1.2(2) ms for nuclear spin 2; see Supplementary Information). **d**,**e**, Electron Ramsey measurements without nuclear spin initialization and with nuclear spin 1 initialized in $|0\rangle_1$ or $|1\rangle_1$ (**d**) and with nuclear spin 1 initialized in $|1\rangle_1$ and nuclear spin 2 in $|0\rangle_2$ or $|1\rangle_2$ (**e**). All error bars and uncertainties in this work are 1σ.

spins by performing nuclear free-evolution experiments (Fig. 2a–d). The oscillations in the expectation values for the X and Y Pauli operators $\langle X\rangle$ and $\langle Y\rangle$ show that the nuclear spins states are successfully read out. The precession frequencies, $\bar{\omega}=2\pi\times 470(1)$ kHz for nuclear spin 1 (Fig. 2c) and $\bar{\omega}=2\pi\times 449(2)$ kHz for nuclear spin 2 (Fig. 2d), are different and agree with the average of $\omega_0=\omega_L$ (for $m_S=0$) and $\omega_1\approx\omega_L+A_\parallel$ (for $m_S=-1$), as expected because the electron spin is continuously flipped ($\omega_L=2\pi\times 431$ kHz is the bare nuclear Larmor frequency). These results confirm that we selectively address the two targeted weakly coupled ^{13}C spins.

Universal control requires both conditional and unconditional gates, while maintaining a high degree of coherence for all qubits in the register. To characterize our gates, we initialize the nuclear spins, prepare the electron spin either in $m_S=0$ or in $m_S=-1$, and apply a gate with a variable number of pulses. For the conditional gate, $\langle Y\rangle$ oscillates in anti-phase for the two electron states: the nuclear spin rotates around the X-axis in a direction that depends on the initial electron state (Fig. 2e). In contrast, for the unconditional gate the rotation direction is independent of the electron state (Fig. 2f). The slow decay of the oscillations indicates that high control fidelities are possible ($F\approx 0.96$ for a single-qubit nuclear $\pi/2$ rotation), enabling us to explore multi-gate sequences that implement nuclear–nuclear gates and quantum error correction.

To realize quantum gates between the nuclear spins[27,30], the mutual interaction of which is negligible, we use the electron spin as a quantum bus. We first verify that both nuclear spins can be prepared and read out in the same experiment by initializing the spins in an eigenstate and performing state tomography by mapping the two-qubit correlations onto the electron spin (Fig. 3a). We then implement entangling gates through an electron controlled gate on nuclear spin 2 and a subsequent coherent SWAP gate between the electron and nuclear spin 1 (Fig. 3b). The tomography reveals strong correlations between the nuclear spins with near-zero single-qubit expectation values, a clear signature of an entangling gate. Despite the 167 electron operations over 986 μs required to implement the five nuclear X-rotations, the fidelity with the target state is 0.66(3) (initialization and readout corrected), demonstrating that the gate can take a pure input state into an entangled state of nuclear spins.

Finally, we implement a quantum-error-correction protocol that protects a quantum state from bit-flip errors by encoding it in a three-qubit state and correcting errors through majority voting (Fig. 4a). Such protocols have been realized with nuclear magnetic resonance[14,15], trapped ions[16] and superconducting qubits[17], but have so far been out of reach for individual solid-state spins due to a lack of multi-qubit control. We compose this protocol from one- and two-qubit gates (Fig. 4b) and separately confirm that the constructed doubly-controlled gate flips the state around the X-axis only if the control qubits (nuclear spins) are in $|1\rangle_1|1\rangle_2$ (Fig. 4c).

We first characterize the effect of errors on each qubit individually. The applied errors are rotations around the X-axis by an angle θ with a random sign (50% clockwise, 50% anticlockwise) and therefore represent a decoherence-type process with a strength determined by θ. We prepare six input states: $|Z\rangle=|0\rangle$, $|-Z\rangle=|1\rangle$, $|\pm X\rangle=(|0\rangle\pm|1\rangle)/\sqrt{2}$ and $|\pm Y\rangle=(|0\rangle\pm i|1\rangle)/\sqrt{2}$ measure the corresponding fidelities F with the output states, and calculate the process fidelity F_p with the identity process

$$F_p=\frac{(F_x+F_{-x}+F_y+F_{-y}+F_z+F_{-z})}{4}-1/2$$

Without error correction, errors on the data qubit (electron spin) are expected to result in an oscillation about $F_{p0}=(F_x+F_{-x})/4$ because only the $|\pm X\rangle$ states are unaffected by the applied errors. With error correction, however, the experimental process fidelity always remains above $F_{p0}=0.293(1)$, even for a completely randomizing error ($\theta=\pi/2$), indicating that the state is partly recovered (Fig. 4d). If one of the ancilla qubits (nuclear spins) is also flipped, an oscillation about F_{p0} is observed; the error correction is effectively turned off because the protocol cannot correct two-qubit errors.

To quantitatively determine the effectiveness of the error correction we analyse it in terms of the three probabilities P_n

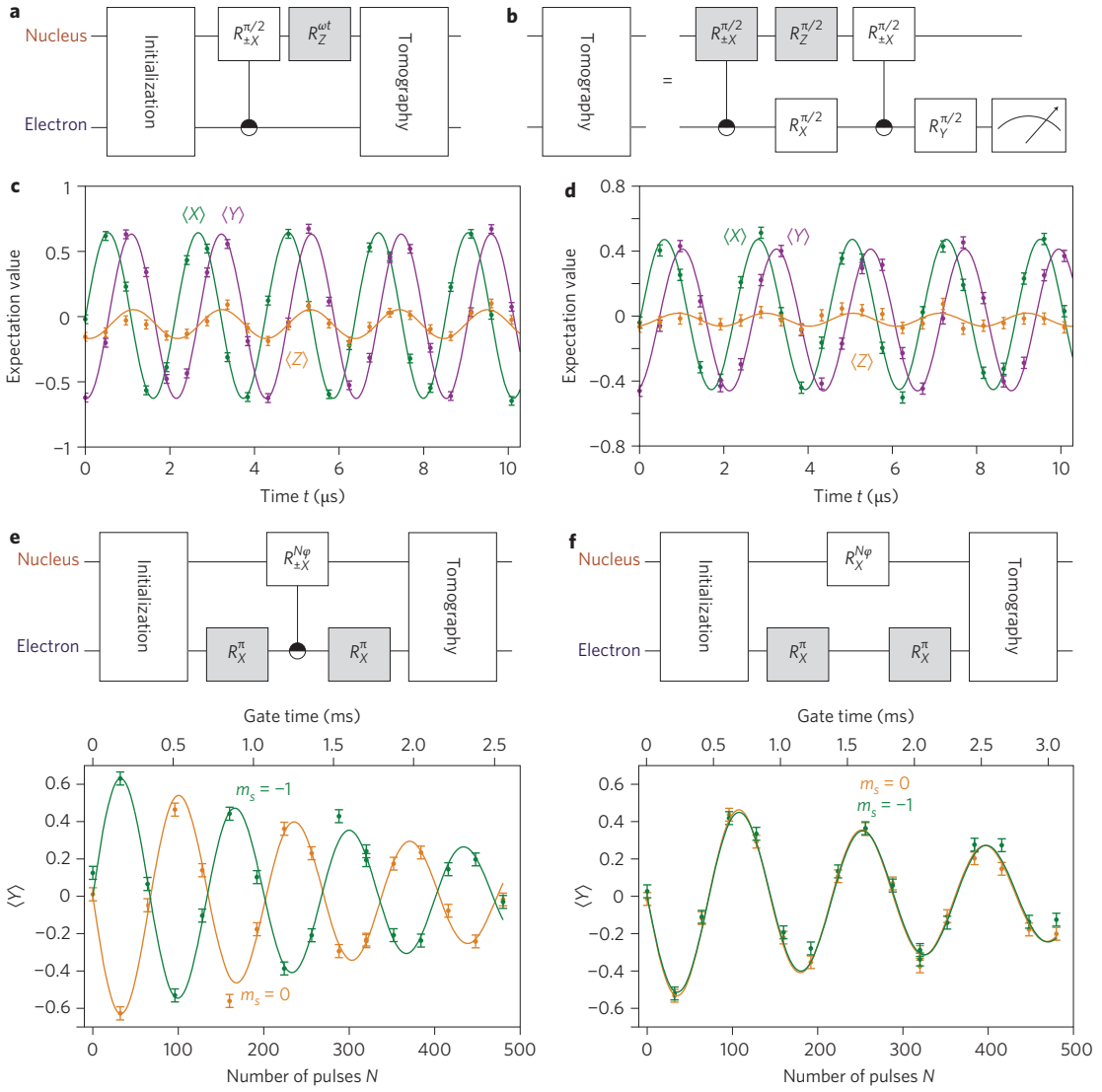

Figure 2 | Individual nuclear spin control and readout. a, Sequence for nuclear-spin free-precession experiments. The *Z*-rotation is implemented by a pulse sequence with off-resonant inter-pulse delay ($\tau = 0.12$ μs) with a variable number of pulses *N*. **b**, Nuclear spin state tomography is performed by mapping the expectation values of the Pauli operators $\langle X\rangle$, $\langle Y\rangle$ and $\langle Z\rangle$ onto the electron spin and reading out the electron (shaded gates are optional basis rotations). **c**,**d**, Measurement of $\langle X\rangle$, $\langle Y\rangle$ and $\langle Z\rangle$ as a function of the free-evolution time. The oscillations in $\langle X\rangle$ and $\langle Y\rangle$ confirm the selective control and readout of the targeted nuclear spins. The amplitude yields a combined readout and initialization fidelity of 0.82(1) for spin 1 (**c**) and 0.72(1) for spin 2 (**d**). Curves are sinusoidal fits. See Supplementary Information for a complete data set with three nuclear spins for each of the three NV centres studied, demonstrating the generality of the control method. **e**, Characterization of the conditional gate for nuclear spin 1. The nuclear spin rotates about the *X*-axis with opposite directions for $m_S = 0$ (without shaded gates) and $m_S = -1$ (with shaded gates). Time for a $\pm\pi/2$ rotation = 170 μs. **f**, Unconditional gate for nucleus 1. Rotation is independent of the electron state. Time for a $\pi/2$ rotation = 254 μs. See Supplementary Information for gates on nuclear spin 2. Results are not corrected for initialization or readout fidelities.

that an applied error on qubit n is successfully corrected and a decoherence/depolarization process during the error-correction protocol itself (see Methods). The model accurately fits the data and gives $P_1 = 0.89(2)$, $P_2 = 0.63(1)$ and $P_3 = 0.84(2)$ for errors on nucleus 1, the electron and nucleus 2, respectively. Crucially, the average probability $\langle P_n\rangle = (P_1 + P_2 + P_3)/3 = 0.786(9)$ is well above 2/3, demonstrating that the process is robust against applied single-qubit errors and that the entropy associated with the errors is successfully shuttled to the ancilla qubits.

We further demonstrate the robustness by applying errors simultaneously on all three qubits (Fig. 4e). Without error correction, that is, without the doubly-controlled gate, a linear dependence is observed and a fit to the expected form gives $\langle P_n\rangle = 0.67(3)$, in excellent agreement with the $\langle P_n\rangle = 2/3$ expected for no robustness to errors. With error correction, a markedly slower initial decay and a nonlinear behaviour with $\langle P_n\rangle = 0.84(3)$ is obtained. This suppression of the linear dependence is a key characteristic of quantum error correction.

The deviation from $\langle P_n\rangle = 1$ is mainly due to imperfect nuclear initialization, which might be improved by repeated initialization steps (see Supplementary Information) or projective measurements[9,21]. We calculate $\langle P_n\rangle = 0.94(2)$ for ideal initialization fidelity (see Supplementary Information). Without applied errors, decoherence and depolarization during the protocol itself (>300 electron operations for 10 nuclear spin gates over 1.8 ms) result in a process fidelity of 0.431(2), corresponding to an average decrease of the state fidelity to 0.93 for one gate (see Supplementary Information). For only the encoding and decoding steps the process fidelity is 0.728(4). The main source of infidelity is electron decoherence ($T_{coh} = 2.86(4)$ ms, Fig. 1b), which is probably

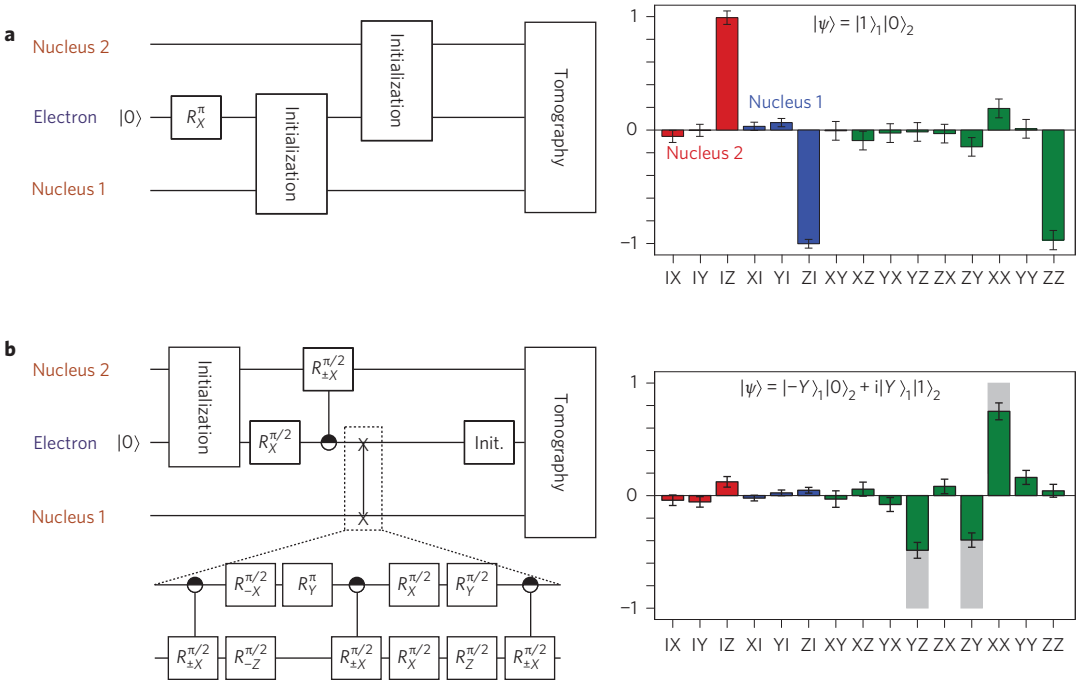

Figure 3 | Two-qubit control and nuclear–nuclear entangling gate. a, The nuclear spins are prepared in $|1\rangle_1|0\rangle_2$ and two-qubit tomography is performed by mapping the 15 combinations of the identity and Pauli operators onto the electron spin (see Supplementary Information). After correction for single-qubit initialization and readout fidelities by renormalizing to the maximum values in Fig. 2c,d, the state fidelity with the target state is $F = 0.99(3)$, indicating that the sequential initialization and two-qubit readout are accurate. **b**, Entangling gate between nuclear spins by coherently swapping the state of the electron onto nuclear spin 1. The nuclear spin coherence is preserved during electron spin re-initialization (a 2 μs laser pulse). T_2^* values under illumination are 51(7) μs and 0.35(9) ms for nuclear spin 1 and 2, respectively (see Supplementary Information). Grey bars depict the target state.

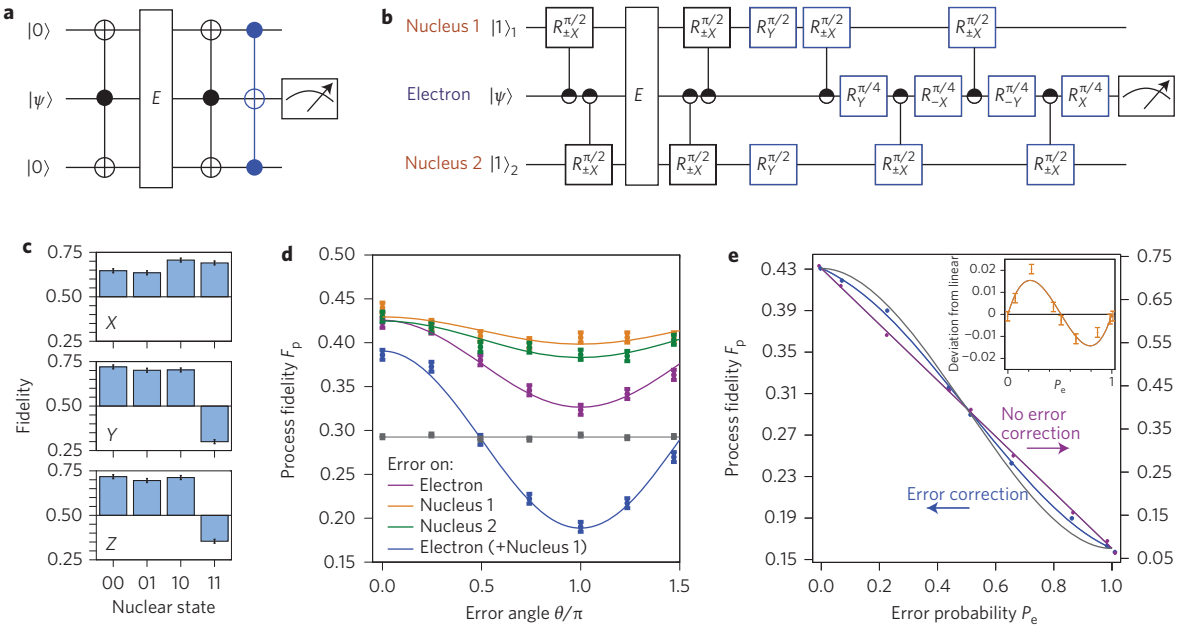

Figure 4 | Implementation of three-qubit quantum error correction. a, Bit-flip quantum-error-correction protocol. State $|\psi\rangle$ is encoded in an entangled state using two ancilla qubits. Potential errors E are detected by decoding and are corrected based on a doubly-controlled NOT gate. **b**, Our implementation of the quantum-error-correction protocol in **a**. The doubly-controlled gate (blue) is constructed using four controlled gates as the final ancilla states are irrelevant. The experiment consists of 308 electron operations in 1.8 ms (excluding initialization). **c**, Characterization of the doubly-controlled gate (blue gates in **b** only). The average output fidelities for $|\pm X\rangle$, $|\pm Y\rangle$ and $|\pm Z\rangle$ are shown for the four ancilla basis states. The average process fidelity with the targeted action is $F_p = 0.534(5)$. **d**, Process fidelity for errors applied to nucleus 1, nucleus 2 or the electron spin (with and without additional flip of nuclear spin 1). Grey data and fit are $F_{p0} = (F_x + F_{-x})/4$, which sets the average value for the expected oscillations if no errors are corrected. **e**, Process fidelity for errors simultaneously applied to all three qubits with error probability P_e. Purple: without error correction. Blue: with error correction. Grey: for ideal robustness against errors. Error bars are given by the symbol size (typical standard deviation 0.002). Inset: deviation of the error correction data from a linear curve. All curves in **d** and **e** are fits to the model in the Methods.

phonon-induced[31] and limits the average fidelity per gate to 0.97. Nuclear spin dephasing further reduces the fidelity to 0.94, close to the observed value (see Supplementary Information). The electronic coherence time is greatly increased at cryogenic temperatures, at which $T_{coh} = 14$ ms (single NV)[18] and $T_{coh} = 0.6$ s (ensembles)[31] have already been reported. Nuclear spin dephasing can be mitigated by decoupling nuclear–nuclear interactions (T_2 measurements are provided in the Supplementary Information). With such future improvements, our results can be used to protect entangled states of solid-state spins.

In conclusion, we have established universal control over weakly coupled nuclear spins that were previously regarded as a source of decoherence. These results provide multiple qubits per defect with high certainty and are compatible with control of the intrinsic nitrogen spin and potential strongly coupled ^{13}C spins. Our techniques can be applied to a wide variety of other electron–nuclear spin systems[2,3,10,13]. The resulting reliable multi-qubit registers can be combined with recently demonstrated coherent coupling between (distant) electron spins[11,18] to realize novel surface-code quantum-computation architectures that use four qubits per defect node[19] and extended quantum networks for long-distance quantum communication.

Note added in proof: After submission of this manuscript, related work by Waldherr *et al.*[32] appeared in which three-qubit quantum error correction is implemented using strongly coupled nuclear spins.

Methods

Diamond sample and hyperfine interactions. We used a room-temperature type II*a* diamond with 1.1% of ^{13}C grown by chemical vapour deposition (Element 6). We applied a magnetic field of $B_z \approx 403$ G along the NV symmetry axis (Z-axis), yielding a ^{13}C Larmor frequency of $\omega_L = 2\pi \times 431$ kHz. The electronic dephasing time T_2^* is 3.3(1) μs. The hyperfine interaction for nuclear spin i is given by $\mathbf{A}_i = A_\parallel^i \hat{\mathbf{z}} + A_\perp^i \hat{\mathbf{x}}$ (Fig. 1a), where $A_\parallel$ is the component parallel to the magnetic field and $A_\perp$ is the perpendicular component. The values determined by dynamical decoupling spectroscopy[23] are $A_\parallel^1 = 2\pi \times 78.2(8)$ kHz and $A_\perp^1 = 2\pi \times 30(1)$ kHz for nuclear spin 1, and $A_\parallel^2 = 2\pi \times 32(3)$ kHz and $A_\perp^2 = 2\pi \times 44(2)$ kHz for nuclear spin 2 (see Supplementary Information). Because $A_\parallel, A_\perp < (2\sqrt{2})/T_2^* = 2\pi \times 136(1)$ kHz, the nuclear spins are weakly coupled to the electron spin and the hyperfine splittings are unresolved.

Nuclear gate design. In a suitable rotating frame, the Hamiltonian with a single nuclear spin can be written as

$$H = |0\rangle\langle 0|H_0 + |1\rangle\langle 1|H_1$$

where $H_0 = \omega_L \hat{I}_Z$ and $H_1 = (\omega_L + A_\parallel)\hat{I}_Z + A_\perp \hat{I}_X$ and $|0\rangle$ and $|1\rangle$ are the $m_S = 0$ and $m_S = -1$ electron states, respectively. Nuclear spin gates were performed by applying sequences of the type $(\tau - \pi - 2\tau - \pi - \tau)^{N/2}$ on the electron spin (Rabi frequency = 31.25 MHz). Because we set $\omega_L \gg A_\perp$, sharp periodic resonances occur at

$$\tau \approx \frac{k\pi}{2\omega_L + A_\parallel}$$

with integer k (see Supplementary Information). At these values, a nuclear X-rotation was performed (assuming $A_\perp \neq 0$). For odd k the direction of the rotation is conditional on the electron spin (for example, the $R_{\pm X}^{\pi/2}$ gates), and for even k it is unconditional ($R_X^{\pi/2}$ gates). We used values of k for which the resonances of the different spins do not overlap. For the conditional gates we took $\tau = 2.656$ μs ($k = 5$), $N = 32$ for spin 1 and $\tau = 3.900$ μs ($k = 7$), $N = 18$ for spin 2. For the unconditional gates we used $\tau = 3.186$ μs ($k = 6$), $N = 40$ for spin 1 and $\tau = 2.228$ μs ($k = 4$), $N = 64$ for spin 2. Z-rotations were implemented by choosing τ to be off-resonant: for values of τ that do not satisfy the above resonance condition the nuclear spins precess unconditionally around the Z-axis with frequency $\bar{\omega} = \omega_L + A_\parallel/2$. Detailed simulations of the nuclear spin dynamics are available in the Supplementary Information.

Nuclear spin initialization. The electron Ramsey measurements in Fig. 1d,e were analysed in two ways. In the first, the measurements were fit separately to

$$F = \frac{1}{2} - \frac{1}{2} e^{-\left(\frac{t}{T_2^*}\right)^2} \cos(\delta t)$$

in which T_2^* is a measure for the dephasing time set by the entire spin bath and δ is the detuning. The external magnetic field stability of better than 2 mG over the total integration time (~2 h), required to measure the increase in T_2^* compared to without nuclear spin initialization, was achieved by post-selecting from a larger measurement set.

In the second, using the hyperfine components $A_\parallel^1$ and $A_\parallel^2$, the measurements were fit to

$$\begin{aligned} F = \frac{1}{2} - 1/2 e^{-(\tau/T_2^{**})^2} \Bigg[& F_1 F_2 \cos\left[\left(\delta + \frac{A_\parallel^1 + A_\parallel^2}{2}\right)t\right] \\ & + F_1(1-F_2)\cos\left[\left(\delta + \frac{A_\parallel^1 - A_\parallel^2}{2}\right)t\right] \\ & + (1-F_1)(F_2)\cos\left[\left(\delta + \frac{-A_\parallel^1 + A_\parallel^2}{2}\right)t\right] \\ & + (1-F_1)(1-F_2)\cos\left[\left(\delta - \frac{A_\parallel^1 + A_\parallel^2}{2}\right)t\right]\Bigg] \end{aligned}$$

where $T_2^{**} = 4.5(3)$ μs is the electronic dephasing due to the rest of the spin bath, that is, not including the two spins under study. To accurately determine the nuclear spin initialization fidelities F_1 and F_2, we used a different data set that was averaged over a longer time (see Supplementary Information).

Quantum error correction analysis. The applied errors realize the quantum map

$$E(\rho, \theta) = \cos^2\frac{\theta}{2} I\rho I + \sin^2\frac{\theta}{2} X\rho X$$

in which ρ is the initial density matrix and I is the identity operator (error characterization in Supplementary Information). We analysed the error-correction protocol by separating depolarization during the encoding, decoding and error-correction steps from the robustness of the encoded state to applied errors, which is characterized by the three probabilities P_n that an error applied on qubit n is successfully corrected (for derivation see Supplementary Information). The process fidelity for a single-qubit error (Fig. 4d) is then given by

$$F_p(\theta) = F_{p0} + A_{YZ}[P_n + (1-P_n)\cos\theta] \quad (1)$$

where $F_{p0} = (F_x + F_{-x})/4$ and $A_{YZ} = (F_y + F_{-y} + F_z + F_{-z} - 2)/4$ characterize the additional depolarization and are given by the average fidelities without applied errors. Equation (1) contains a constant due to the $|\pm X\rangle$ states, which are unaffected by the applied error, and a sum of successful ($P_n = 1$) and unsuccessful ($P_n = 0$) error correction for the $|\pm Y\rangle$ and $|\pm Z\rangle$ states. For errors simultaneous on all three qubits (Fig. 4e), the process fidelity becomes

$$\begin{aligned} F_p(P_e) = F_{p0} + A_{YZ}[1 - 3P_e + 3P_e^2 - 2P_e^3 \\ + 3(2\langle P_n\rangle - 1)(P_e - 3P_e^2 + 2P_e^3)] \end{aligned}$$

where $P_e = \sin^2(\theta/2)$ is the error probability. In general, this equation describes a third-order polynomial. For ideal error correction ($\langle P_n\rangle = 1$) the linear term vanishes, whereas without robustness to errors, $\langle P_n\rangle = 2/3$, the result is strictly linear. The inversion symmetry about $P_e = 0.5$ observed both theoretically and experimentally ensures that the nonlinear behaviour is not due to spurious coherent rotations.

Received 15 September 2013; accepted 7 January 2014; published online 2 February 2014; corrected online 7 February 2014

References

1. Awschalom, D. D., Bassett, L. C., Dzurak, A. S., Hu, E. L. & Petta, J. R. Quantum spintronics: engineering and manipulating atom-like spins in semiconductors. *Science* **339,** 1174–1179 (2013).
2. Koehl, W. F., Buckley, B. B., Heremans, F. J., Calusine, G. & Awschalom, D. D. Room temperature coherent control of defect spin qubits in silicon carbide. *Nature* **479,** 84–87 (2011).
3. Yin, C. *et al.* Optical addressing of an individual erbium ion in silicon. *Nature* **497,** 91–94 (2013).
4. Gurudev Dutt, M. V. *et al.* Quantum register based on individual electronic and nuclear spin qubits in diamond. *Science* **316,** 1312–1316 (2007).
5. Neumann, P. *et al.* Multipartite entanglement among single spins in diamond. *Science* **320,** 1326–1329 (2008).
6. Fuchs, G. D., Burkard, G., Klimov, P. V. & Awschalom, D. D. A quantum memory intrinsic to single nitrogen–vacancy centres in diamond. *Nature Phys.* **7,** 789–793 (2011).

7. Van der Sar, T. *et al.* Decoherence-protected quantum gates for a hybrid solid-state spin register. *Nature* **484,** 82–86 (2012).
8. Maurer, P. C. *et al.* Room-temperature quantum bit memory exceeding one second. *Science* **336,** 1283–1286 (2012).
9. Pfaff, W. *et al.* Demonstration of entanglement-by-measurement of solid-state qubits. *Nature Phys.* **9,** 29–33 (2013).
10. Pla, J. J. *et al.* High-fidelity readout and control of a nuclear spin qubit in silicon. *Nature* **496,** 334–338 (2013).
11. Dolde, F. *et al.* Room-temperature entanglement between single defect spins in diamond. *Nature Phys.* **9,** 139–143 (2013).
12. Jiang, L. *et al.* Repetitive readout of a single electronic spin via quantum logic with nuclear spin ancillae. *Science* **326,** 267–272 (2009).
13. Lee, S-Y. *et al.* Readout and control of a single nuclear spin with a metastable electron spin ancilla. *Nature Nanotech.* **8,** 487–492 (2013).
14. Cory, D. G. *et al.* Experimental quantum error correction. *Phys. Rev. Lett.* **81,** 2152–2155 (1998).
15. Moussa, O., Baugh, J., Ryan, C. A. & Laflamme, R. Demonstration of sufficient control for two rounds of quantum error correction in a solid state ensemble quantum information processor. *Phys. Rev. Lett.* **107,** 160501 (2011).
16. Schindler, P. *et al.* Experimental repetitive quantum error correction. *Science* **332,** 1059–1061 (2011).
17. Reed, M. D. *et al.* Realization of three-qubit quantum error correction with superconducting circuits. *Nature* **482,** 382–385 (2012).
18. Bernien, H. *et al.* Heralded entanglement between solid-state qubits separated by three metres. *Nature* **497,** 86–90 (2013).
19. Nickerson, N. H., Li, Y. & Benjamin, S. C. Topological quantum computing with a very noisy network and local error rates approaching one percent. *Nature Commun.* **4,** 1756 (2013).
20. Neumann, P. *et al.* Single-shot readout of a single nuclear spin. *Science* **329,** 542–544 (2010).
21. Robledo, L. *et al.* High-fidelity projective read-out of a solid-state spin quantum register. *Nature* **477,** 574–578 (2011).
22. Dreau, A., Spinicelli, P., Maze, J. R., Roch, J. F. & Jacques, V. Single-shot readout of multiple nuclear spin qubits in diamond under ambient conditions. *Phys. Rev. Lett.* **110,** 060502 (2013).
23. Taminiau, T. H. *et al.* Detection and control of individual nuclear spins using a weakly coupled electron spin. *Phys. Rev. Lett.* **109,** 137602 (2012).
24. Kolkowitz, S., Unterreithmeier, Q. P., Bennett, S. D. & Lukin, M. D. Sensing distant nuclear spins with a single electron spin. *Phys. Rev. Lett.* **109,** 137601 (2012).
25. Zhao, N. *et al.* Sensing single remote nuclear spins. *Nature Nanotech.* **7,** 657–662 (2012).
26. Hodges, J. S., Yang, J. C., Ramanathan, C. & Cory, D. G. Universal control of nuclear spins via anisotropic hyperfine interactions. *Phys. Rev. A* **78,** 010303 (2008).
27. Zhang, Y., Ryan, C. A., Laflamme, R. & Baugh, J. Coherent control of two nuclear spins using the anisotropic hyperfine interaction. *Phys. Rev. Lett.* **107,** 170503 (2011).
28. Maze, J. R., Taylor, J. M. & Lukin, M. D. Electron spin decoherence of single nitrogen–vacancy defects in diamond. *Phys. Rev. B* **78,** 094303 (2008).
29. London, P. *et al.* Detecting and polarizing nuclear spins with double resonance on a single electron spin. *Phys. Rev. Lett.* **111,** 067601 (2013).
30. Filidou, V. *et al.* Ultrafast entangling gates between nuclear spins using photoexcited triplet states. *Nature Phys.* **8,** 596–600 (2012).
31. Bar-Gill, N., Pham, L. M., Jarmola, A., Budker, D. & Walsworth, R. L. Solid-state electronic spin coherence time approaching one second. *Nature Commun.* **4,** 1743 (2013).
32. Waldherr, G. *et al.* Quantum error correction in a solid-state hybrid spin register. Preprint at http://arxiv.org/abs/1309.6424 (2013).

Acknowledgements

The authors thank L. Childress, J.J.L. Morton, O. Moussa and L.M.K. Vandersypen for discussions and comments. T.H.T. acknowledges support from a Marie Curie Intra European Fellowship within the 7th European Community Framework Programme. Work at the Ames Laboratory was supported by the US Department of Energy Basic Energy Sciences (contract no. DE- AC02-07CH11358). The authors acknowledge support from the Dutch Organization for Fundamental Research on Matter (FOM), the Netherlands Organization for Scientific Research (NWO), the DARPA QuASAR programme, the EU SOLID and DIAMANT programmes, and the European Research Council through a Starting Grant.

Author contributions

V.V.D., T.H.T., T.v.d.S. and R.H. conceived the control method. T.H.T., J.C., T.v.d.S. and R.H. devised the experiments. T.H.T., J.C. and T.v.d.S. performed the measurements and processed the data. T.H.T. and R.H. wrote the manuscript. All authors analysed the results and commented on the manuscript.

Additional information

Supplementary information is available in the online version of the paper. Reprints and permissions information is available online at www.nature.com/reprints. Correspondence and requests for materials should be addressed to R.H.

Competing financial interests

The authors declare no competing financial interests.

ERRATUM

Universal control and error correction in multi-qubit spin registers in diamond

T. H. Taminiau, J. Cramer, T. van der Sar, V. V. Dobrovitski and R. Hanson

Nature Nanotechnology http://dx.doi.org/10.1038/nnano.2014.2 (2014); published online 2 February 2014;
corrected online 7 February 2014.

In the version of this Letter originally published online, in Fig. 3b in one instance of $R_X^{\pi/2}$, a subscript '*a*' was used instead of a subscript '*X*'. This error has now been corrected in all versions of the Letter.